PCCP

PAPER

View Article Online
View Journal | View Issue

Cite this: *Phys. Chem. Chem. Phys.*, 2022, **24**, 17569

Coincidence ion pair production (cipp) spectroscopy of diiodine†

Kristján Matthíasson, [a] Ágúst Kvaran, *[a] Gustavo A. Garcia, [b] Peter Weidner [c] and Bálint Sztáray *[c]

Received 11th April 2022, Accepted 27th June 2022

DOI: 10.1039/d2cp01684b

rsc.li/pccp

Coincidence ion pair production ($I^+ + I^-$) (cipp) spectra of I_2 were recorded in a double imaging coincidence experiment in the one-photon excitation region of 71 600–74 000 cm^{-1}. The $I^+ + I^-$ coincidence signal shows vibrational band head structure corresponding to iodine molecule Rydberg states (I_2^{**}) crossing over to ion-pair (I^+I^-) potential curves above the dissociation limit. The band origin (ν^0), vibrational wavenumber (ω_e) and anharmonicity constants ($\omega_e x_e$) were determined for the identified Rydberg states. The analysis revealed a number of previously unidentified states and a reassignment of others following a discrepancy in previous assignments. Since the ion pair production threshold is well established, the electric field-dependent spectral intensities were used to derive the cutoff energy in the transitions to the rotational levels of the 7pσ(1/2) (v' = 3) state.

I. Introduction

A large number of Rydberg states have been identified for the iodine molecule (I_2) by standard absorption spectroscopy[1] and by REMPI.[2–4] Interactions between Rydberg and ion-pair states are well known for the halogens[5–9] as well as for the interhalogens.[10–12] These have been found to occur either above or below[7,8,12,13] the dissociation energy thresholds for ion-pair states. In the former case, ion pairs ($AB \rightarrow A^+ + B^-$) are formed by bound Rydberg-to-free ion-pair state transitions, whereas in the latter case bound-to-bound (Rydberg to ion-pair state) state transfer occurs. Exciting I_2 into a bound high energy Rydberg state which interacts with an ion-pair state should simultaneously form positive and negative ions, I^+ and I^- at discreet energies once the excitation energy goes above the respective ion-pair dissociation energy threshold.[14,15] Kvaran *et al.* demonstrated this by vibrationally resolved excitation of I_2, where both I^+ and I^- were formed above the dissociation threshold of about 72 150 cm^{-1}.[6] They observed virtually identical ion yield spectra for both atomic ions (I^+ and I^-) in the excitation region above the ion pair threshold. Spectral analysis revealed series of overlapping Rydberg states converging to the molecular ion ground state.

Recently, we have used the new experimental technique of coincidence ion pair production (cipp) spectroscopy, which is based on the coincident detection of the positive and negative ions that are formed together. Experimentally, the cipp setup is identical to the well-established technique of photoelectron photoion coincidence (pepico) spectroscopy (bar some trivial wiring details). In the first such work, we have measured molecular fluorine (F_2) and shown that cipp signal shows rotational band head structure, corresponding to F_2 Rydberg states crossing over to the ion pair production potential surface. Spectral simulation and quantum defect analysis allowed characterization of five new molecular Rydberg states. The lowest-energy observed Rydberg state lacked some of the predicted rotational structure, which allowed an accurate determination of the ion pair production threshold which, together with pepico experiments carried out on the same apparatus, allowed us to determine the previously disputed F_2 dissociation energy with unprecedented accuracy.[16]

In this paper, we present coincidence ion pair production (cipp) spectra for I_2, which allowed identification of a large number of Rydberg states. Detailed analyses of the spectra and reanalysis of older absorption data[1] revealed a number of new states and complete reassignment of some I_2 molecule Rydberg states. Furthermore, detailed spectral simulations revealed how the cipp spectral intensities vary with the electric field near the ion pair formation energy threshold.

II. Experimental

The experiments were carried out with the DELICIOUS III double-imaging photoelectron photoion coincidence (i^2PEPICO)

[a] *Science Institute, University of Iceland, Dunhagi 3, 107 Reykjavík, Iceland. E-mail: agust@hi.is*
[b] *Synchrotron SOLEIL, L'Orme des Merisiers, St, Aubin BP 48, 91192 Gif sur Yvette, France*
[c] *Department of Chemistry, University of the Pacific, Stockton, CA-95211, USA. E-mail: bsztaray@pacific.edu*

† Electronic supplementary information (ESI) available. See DOI: **https://doi.org/10.1039/d2cp01684b**

spectrometer on the DESIRS undulator beamline[17] of Synchrotron Soleil, in France. The instrument has been described in detail elsewhere[18] and only a brief summary of the relevant parts is given here. Briefly, crystals of iodine were sublimated in an oven kept at 80 °C in a stream of helium bath gas. The iodine gas entered the ionization chamber through a supersonic expansion of an I_2/He mixture, through a 200 μm heated nozzle, kept at 90 °C. The supersonic beam was collimated with a double skimmer setup of the SAPHIRS molecular beam endstation.[19] Typical pressures were 1.5×10^{-3} mbar in the expansion, 3.5×10^{-6} mbar in the differential pumping, and less than 9×10^{-8} mbar in the ionization regions. Photons from the variable polarization undulator OPHELIE2 were dispersed by a 6.65 m normal-incidence monochromator with a 2400 lines per mm grating and focused onto a 200/300 μm (H/V) spot in the ionization region. The entrance and exit slits of the monochromator were set to 100 μm and 300 μm, respectively, providing an energy resolution of 9.7 cm^{-1} (1.2 meV) at 130 000 cm^{-1} (16 eV). To block out high-order harmonics, a gas filter located upstream of the beamline was filled with neon. For absolute energy calibration, the same gas filter was filled with krypton and its well-known absorption lines, corresponding to dips in the cation signal, because of the diminished photon intensity due to absorption by krypton in the gas filter, were used for calibration. Specifically, the $4p^5(^2P^\circ_{3/2})5s{-}4p^6(^1S)$ (80 916.75 cm^{-1}) and $4p^5(^2P^\circ_{1/2})5s'{-}4p^6(^1S)$ (85 846.71 cm^{-1}) absorption lines were used for calibration as reported by Yoshino and Tanaka and later deposited into the NIST Atomic Spectra Database.[20,21] To validate the accuracy of this calibration, the cipp spectral lines were cross-referenced against the Venkateswarlu spectra,[1] *vide infra*.

The DELICIOUS III spectrometer is composed of an electron velocity map imaging setup and a modified Wiley–McLaren time-of-flight 3D momentum imaging ion mass analyzer in a multistart–multistop coincidence detection mode. This setup produces a multi-dimensional coincidence data set, two cross sections of which yield photoion mass-selected photoelectron spectra, as well as mass spectra of internal energy-selected photoions. In the recently pioneered coincidence ion pair production (cipp) experiments, the same physical setup was utilized, except that anions were detected on the imaging electron detector, in coincidence with cations from the same ion pair production events, as explained in more detail in the first cipp publication.[16] Ion pair production coincidences were registered at the calculated and experimentally confirmed time delay between the I^+ and I^- ions, using raytracing simulations of the DELICIOUS III coincidence setup.

III. Results and analysis

The coincidence ion pair production experiments were carried out in an electric field and, as previously noted,[16] the cipp spectral lines may be susceptible to Stark shifts. Therefore, the experiments were carried out at three different extraction fields: 17.7, 44.3, and 88.7 V cm^{-1}. Due to limitations on the available synchrotron beamtime, the whole spectral range (8.92–9.17 eV) was only covered in the 44.3 V cm^{-1} measurements. The 17.7 V cm^{-1} measurements were carried out in the 8.92–9.06 eV range. In order to assess the effect of higher electric field near the ion pair production threshold, we have also collected data with 88.7 V cm^{-1} field for the first 40 meV of the spectra. Fig. 1 shows the collected cipp spectra at the three extraction fields and a cursory comparison shows that, unlike

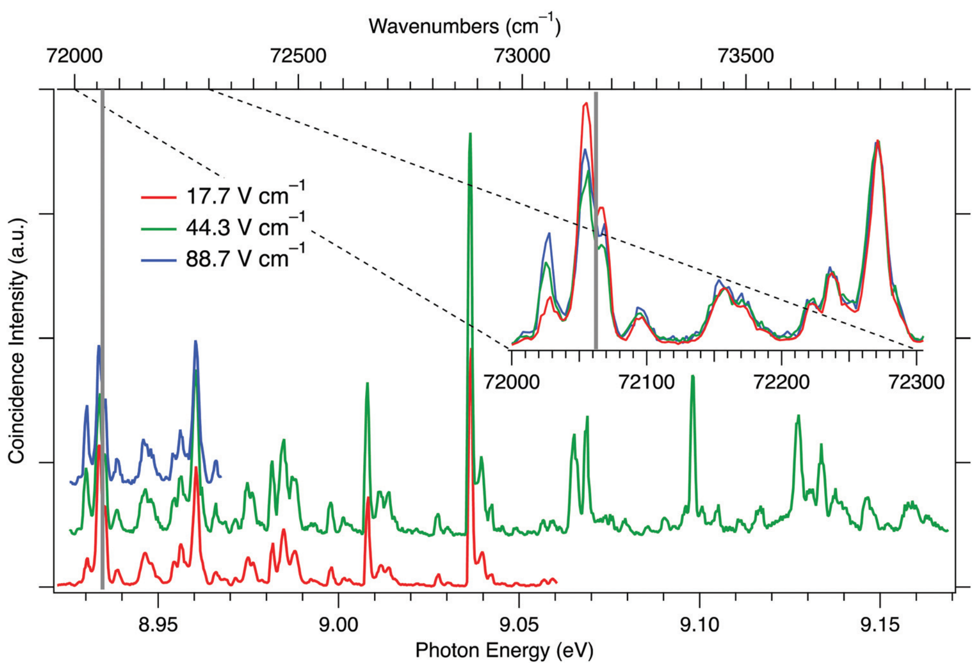

Fig. 1 The effect of the extraction field strength on the cipp spectra. Main graph shows the collected cipp data at three electric fields and the inset shows the magnified low-energy part near the ion pair production threshold. Vertical gray lines show the zero-field ion pair production threshold.

the F_2 cipp spectra,[16] the peaks do not shift significantly with the extraction field strengths. However, close to the ion pair production threshold, the peak intensities and peak shapes do exhibit field-dependence. The inset in Fig. 1 shows that the first major peak between 72 020–72 030 cm^{-1} is diminished at low field, while the next peak and its shoulder between 72 045–72 065 cm^{-1} is somewhat enhanced, when the spectra are normalized for matching peak intensities above 72 100 cm^{-1}.

Spectral analysis

The mid-field (44.3 V cm^{-1}) spectrum was used for spectral analysis. It is shown in Fig. 1 and 2 for the excitation region of 71 600–74 000 cm^{-1}. These show vibrational spectral bands due to transitions from the ground state I_2, $X^1\Sigma^+(v'' = 0)$ to Rydberg vibrational states $\left(I_2^{**}(v')\right)$ followed by a transfer to an ion-pair state (I^+I^-) above its dissociation limit to form I^+ and I^-, *i.e.*,

$$I_2 + h\nu \rightarrow I_2^{**}(v'); \quad \text{photoexcitation} \tag{1a}$$

$$I_2^{**} \rightarrow I^+I^-; \quad \text{state transfer} \tag{1b}$$

$$I^+I^- \rightarrow I^+ + I^-; \quad \text{dissociation} \tag{1c}$$

No signal was detected below 71 730 cm^{-1} and the weak spectral bands in the region of 71 730–71 930 cm^{-1} are "hot bands" due to transitions from $v'' = 1$ (see Fig. 2). This is in agreement with expectations, since the threshold for atom ion pair (I^+/I^-) formation is predicted to be 72 062.4 ± 0.5 cm^{-1}.[22] These spectral bands show close correspondence to peak positions observed in the absorption spectra by Venkateswarlu.[1] The published peak assignment therein, however, needed a revision based on a quantum defect analysis in combination with a spectral simulation.

The band origin (ν_0^0) of a Rydberg vibrational state $\left(I_2^{**}(v')\right)$ spectrum due to transitions to the lowest vibrational level, $v' = 0$ can, to a first approximation, be expressed as,

$$\nu_0^0([\Omega_c]nl\lambda) = \mathrm{IE}([\Omega_c]) - \frac{R_\infty}{(n-\delta_l)^2} \tag{2}$$

where $[\Omega_c]nl\lambda$ refers to a Rydberg state which converges to either of the two spin–orbit components $\left(\Omega_c = \frac{3}{2}, \frac{1}{2}\right)$ of the ground ionic state $I_2^+(X^2\Pi_g)$ in vibrational level $v^+ = 0$, for a Rydberg electron with principal quantum number n, in a molecular orbital λ, corresponding to an atomic orbital l. $\mathrm{IE}([\Omega_c])$ is the ionization energy of $I_2(X^1\Sigma_g^+(v'' = 0, J'' = 0))$ to form $I_2^+([\Omega_c])$ for $v^+ = 0$. R_∞ is the Rydberg constant (109 735.85 cm^{-1}) and δ_l is an l-dependent quantum defect value, which is a measure of how much a Rydberg series diverges from the corresponding hydrogen atom Rydberg series. The I_2 molecule is best described by Hunds case (c)[23] in which case the total spin is not a good quantum number and singlet and triplet states are not distinguishable. Accepted values for the

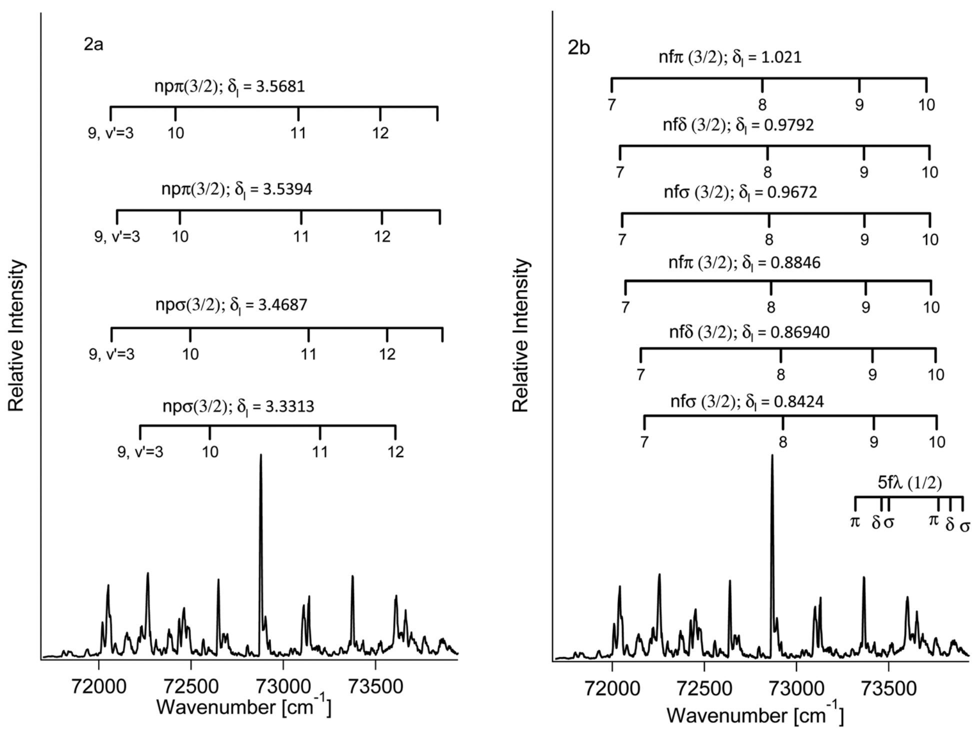

Fig. 2 Coincidence ion pair production spectra of I_2 for the one-photon excitation region of 71 700–74 000 cm^{-1} with assignments. (a) Vibrational band head assignments for the p series Rydberg states converging to the 3/2 spin–orbit ground state ion core. Lowest-energy vibrational quantum numbers (v'_{min}), when larger than zero (v') are marked. (b) Vibrational band head assignments for the f series Rydberg states converging to the 3/2 spin–orbit ground state ion core and assignment of the 5f orbital converging to the 1/2 spin–orbit ground state ion core.

ionization energies of I_2 to form $I_2^+\left(\left[\Omega_c = \frac{3}{2}\right]\right)$ of 9.3074 ± 0.0002 eV (75 069 cm^{-1}) and to form $I_2^+\left(\left[\Omega_c = \frac{1}{2}\right]\right)$ of 9.950 ± 0.002 eV (80 252 cm^{-1})[22,24] were used. These differ significantly from the 9.3995 eV (75 814 cm^{-1}) and 10.0297 eV (80 895 cm^{-1}) values, respectively, used by Venkateswarlu,[1] which explains why the overall Rydberg state assignments needed to be revised. δ_l values of about 3.5 ± 0.1 and 0.93 ± 0.12 were reported by Venkateswarlu for $p(l = 1)$ and $f(l = 3)$ Rydberg

Table 1 Calculated and observed band origins (ν_0^0) based on quantum defect analysis (see eqn (1)) for spectral bands/peaks from the work of Venkateswarlu[1] and ours (*), (a) *n*p Rydberg series converging to the Ω = 3/2 and 1/2 ionic states, (b) *n*f Rydberg series converging to the Ω = 3/2 and 1/2 states of I_2^+

(a)

	*n*p (3/2); δ_l = 3.3313		*n*p (3/2); δ_l = 3.4687		*n*p (3/2); δ_l = 3.5394		*n*p (3/2); δ_l = 3.56812	
n	Calculated	Observed	Calculated	Observed	Calculated	Observed	Calculated	Observed
6	59 660	59 662	57 942	57 958	56 944	56 944	56 613	56 519
7	66 916	66 948	66 269	66 310	65 906	65 951	65 752	65 736
8	70 034	70 028	69 725	69 717	69 554	69 558	69 482	69 486
9	71 654	71 654	71 482	71 485	71 389	71 389	71 350	71 350
10	72 601	72 602*	72 497	72 496*	72 440	72 440*	72 416	72 416*
11	73 203	73 200*	73 135	73 138*	73 098	73 098*	73 082	73 085*
12	73 608	73 608*	73 562	73 563*	73 536	73 535*	73 526	73 525*
13	73 895	73 893	73 861	73 863	73 843	73 849	73 836	73 835
14	74 105	74 106	74 080	74 081	74 066	—	74 061	—
15	74 263	—	74 244	74 234	74 234	74 234	74 230	—
16	74 385	—	74 370	74 367	74 363	74 364	74 359	74 355
17	74 481	74 484	74 470		74 464	74 465	74 461	74 465
18	74 559	—	74 550		74 544	—	74 542	—
19	74 622	71 622	74 614		74 610	—	74 608	—
20	74 674	74 672	74 668		74 664	—	74 663	—
21	74 717	—	74 712		74 709	74 079	74 708	74 709
22	74 754	74 756	74 750		74 747	—	74 746	

	*n*p (1/2); δ_l = 3.3313		*n*p (1/2); δ_l = 3.4687		*n*p (1/2); δ_l = 3.5394		*n*p (1/2); δ_l = 3.56812	
n	Calculated	Observed	Calculated	Observed	Calculated	Observed	Calculated	Observed
6	64 841	64 803	63 122	63 122	62 124	62 144	61 694	91 722
7	72 096	72 096*	71 449	71 449	71 086	71 085	70 932	70 930
8	75 215	75 214	74 904	74 906	74 733	74 767	74 662	74 672

(b)

	*n*f (3/2); δ_l = 0.84243		*n*f (3/2); δ_l = 0.8636		*n*f (3/2); δ_l = 0.8846		*n*f (3/2); δ_l = 0.9672		*n*f (3/2); δ_l = 0.9861		*n*f (3/2); δ_l = 1.021	
n	Calculated	Observed	Calculated	Observed	Calculated	Observed	Calculated	Observed	Calculated	Observed	Calculated	Observed
4	64 063	64 074	63 914	63 930	63 763	63 754	63 138	63 122	62 988	63 004	62 705	62 696
5	68 721	68 733	68 656	68 652	68 590	68 605	68 322	68 325	68 258	68 179	68 139	68 159
6	70 944	70 955	70 910	70 918	70 876	70 883	70 737	70 730	70 704	70 702	70 643	70 637
7	72 175	72 175*	72 155	72 155*	72 135	72 135*	72 054	72 054*	72 035	72 035*	72 000	72 000
8	72 927	72 930*	72 915	72 914*	72 902	72 901*	72 851	72 850*	72 839	72 839*	72 816	72 815*
9	73 420	73 422*	73 412	73 411*	73 403	73 403*	73 369	73 368*	73 361	73 360*	73 346	73 341*
10	73 761	73 762*	73 755	73 750*	73 749	73 748*	73 724	73 724*	73 719	73 719*	73 708	73 705*
11	74 005	74 010	74 001	73 999	73 997	73 999	73 979	73 984	73 975	73 967	73 967	73 967
12	74 188	—	74 184	—	74 181	—	74 168	74 167	74 165	74 167	74 159	74 157
13	74 327	74 328	74 324	—	74 322	—	74 311	74 311	74 309	74 311	74 305	—
14	74 435	—	74 433	74 431	74 431	74 431	74 423	74 423	74 421	74 423	74 418	74 414
15	74 522	74 521	7452	74 521	74 518	74 513	74 512	74 513	74 510	74 513	74 508	74 513
16	74 592	74 590	74 590	74 590	74 589	74 590	74 584	74 577	74 582	74 577	74 580	74 577
17	74 649	74 646	74 648	74 676	74 647	74 646	74 642	74 642	74 641	74 642	74 639	74 642
18	74 696	74 697	74 696	74 694	74 695	74 694	74 691	74 694	74 690	74 694	74 689	—
19	74 736	74 735	74 736	74 735	74 735	—	74 732	74 735	74 731	74 735	74 730	74 723
20	74 770	74 767	74 770	74 767	74 769	74 767	74 766	74 767	74 766	74 762	74 765	74 767
21	74 799	74 797	74 799	74 797	74 798	74 797	74 796	74 797	74 795	74 797	74 794	74 797
22	74 824	74 823	74 824	74 823	74 823	74 823	74 821	74 823	74 821	74 823	74 820	74 823

	*n*f (1/2); δ_l = 0.84243		*n*f (1/2); δ_l = 0.8636		*n*f (1/2); δ_l = 0.8846		*n*f (1/2); δ_l = 0.9672		*n*f (1/2); δ_l = 0.9861		*n*f (1/2); δ_l = 1.021	
n	Calculated	Observed	Calculated	Observed	Calculated	Observed	Calculated	Observed	Calculated	Observed	Calculated	Observed
4	69 243	69 256	69 052	69 053	68 943	68 845	68 318	68 325	68 168	68 165	68 139	68 159
5	73 901	73 904*	73 818	73 814*	73 769	73 769*	73 502	73 501*	73 438	73 438*	73 319	73 319*

series of I_2[1] and judging from atomic energy levels[25] δ_l values of about 4.01, 3.57, 2.50 and 0.04 are expected for s(l = 0), p(1), d(2) and f(3) Rydberg electron iodine atom orbitals, respectively.

Determination of the band origins (ν_0^0) was based on a search of band/peak series observed in our spectra as well as the absorption spectra[1] for consistent and realistic values of δ_l (*i.e.* a quantum defect analysis). The experimental band/peak maxima were assumed to correspond to the band origin. This could be justified for our observed spectral bands by analysis of band shapes (see Fig. S1 and S2 in the ESI†). A total of 20 Rydberg state series were identified (see Table 1 and Fig. 2). Eight Rydberg series were found to correspond to transitions to *n*p Rydberg orbitals (δ_l in the range of 3.33–3.57), for which four converge to the Ω_c = 3/2 spin–orbit molecular ion state and four converge to the Ω_c = 1/2 spin–orbit excited state. Further 12 Rydberg series were found to correspond to transitions to *n*f Rydberg orbitals (δ_l in the range of 0.84–1.03), with six series converging to each of the two spin–orbit ion states.

The λ(σ, π, or δ) configurations of the Rydberg states were further specified by energetic considerations based on,

(i) that the energy progression of Rydberg molecular states is analogous to that of the corresponding Rydberg atomic states, for s < p < d < f.

(ii) that the energies change as π < δ < σ for the f Rydberg series and as π < σ for the p series.[23]

Thus, series of f(σ, π, δ) and p(σ, π) states were identified as listed in Table 1. Two series for each set of quantum numbers were identified due to the two possible spin states of the excited electron. Energy differences corresponding to the spin–orbit coupling for the p and f Rydberg electrons were found to be about 330 cm^{-1} and 1000 cm^{-1}, respectively, virtually independent of λ(σ, π, δ) for the same l (f or p). Judging from our observations the trends in (i)–(ii) are independent of the molecular ion core spin–orbit configuration ([1/2], [3/2]).

In combination with the quantum defect analysis of the band origins for ν' = 0(ν_0^0), search for vibrational bands due to transitions to higher Rydberg vibrational states ($\nu_{\nu'}^0$; ν' > 0) was made (Fig. 3). This was guided by the assumption that the vibrational frequencies/wavenumbers are comparable to that of the ground neutral ($\omega_e'' = 214.50$ cm^{-1} [22]) and ionic (ω_e^+ = 220–240 cm^{-1} [22]) molecular states. Finally, the observed spectrum was simulated by using the PGOPHER program.[26] The simulation was performed by optimizing a fit of calculated and experimental spectra for the total spectral range. The calculated spectra were based on Franck–Condon factors for the absorption transition, using known vibrational constants for the ground state of I_2 and vibrational constants for the excited states as fit parameters. Voigt (a combination of Gaussian width contribution of 8 cm^{-1} and Lorentzian width contribution of 2 cm^{-1}) line profiles were used to represent the vibrational bands profiles (see Fig. 3 and 4). The fit analysis resulted in vibrational temperature (T_{vib}) of about 40 K. In some cases, significant difference in peak intensities was observed between the experimental and calculated spectra. This is not a surprise, since the cipp detection depends on the crossover from the Rydberg states to ion-pair states, in addition to absorption, whereas the simulation is based on the absorption

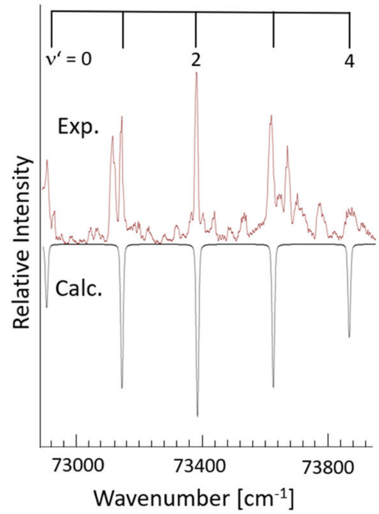

Fig. 3 Vibrational simulation of the transition from the ground state to the 8fδ$_u$ state. Experimental spectrum on top (red). Calculated spectrum (black, bottom) formed by using a combination of Gaussian line widths of 8 cm^{-1} and Lorentzian line widths of 2 cm^{-1} (see main text), vibrational temperature of T = 40 K, and spectroscopic values of ω_e = 238 cm^{-1} and $\omega_e x_e$ = 0.6 cm^{-1}.

cross-sections only. In particular we were unable to fit/explain an unusually high intensity peak which appears at 72 874 cm^{-1} (see Fig. 4).

All in all, the analyses allowed assignment of the Rydberg state spectra with respect to n, l, λ and ν' as well as determination of band origin (ν_0^0), vibrational wavenumber (ω_e), and in some cases anharmonicity constants ($\omega_e x_e$) for the Rydberg states (see Tables 1 and 2).

Ion pair threshold energetics

Close-up figure in the threshold energy region reveals missing vibrational bands below 72 020 cm^{-1} (Fig. 4b). The lack of observable lines in that region must correspond to transitions with energy levels below the ion pair dissociation energy threshold for I_2. The Active Thermochemical Tables (ATcT) value of the ion pair production threshold is 862.0575 ± 0.0061 kJ mol^{-1} or 72062.4 ± 0.5 cm^{-1},[27] which is significantly larger than the observed cut off in our cipp spectra (≤72 030 cm^{-1}). This must be due to a shifting of the ion pair production threshold by the applied electric field in the extraction region of the spectrometer. The ion pair production threshold is known to red-shift in energy (ΔE) proportionally to the square root of the electric field (F) as,

$$\Delta E = \alpha\sqrt{F}$$

were α is the shift constant.[28–31] Typical measured values of α range from −3.9 to −6.11 cm^{-1}, when F is given in V cm^{-1}.[32]

The relative intensity of the spectral band at 72 025 cm^{-1} is found to increase with the electric field (F) (see Fig. 1 and 5). This can be attributed to a different cutoff of the rotational energy levels of the 7pσ(1/2) (ν' = 3) vibrational Rydberg state, as the ion pair energy threshold decreases with increasing F.

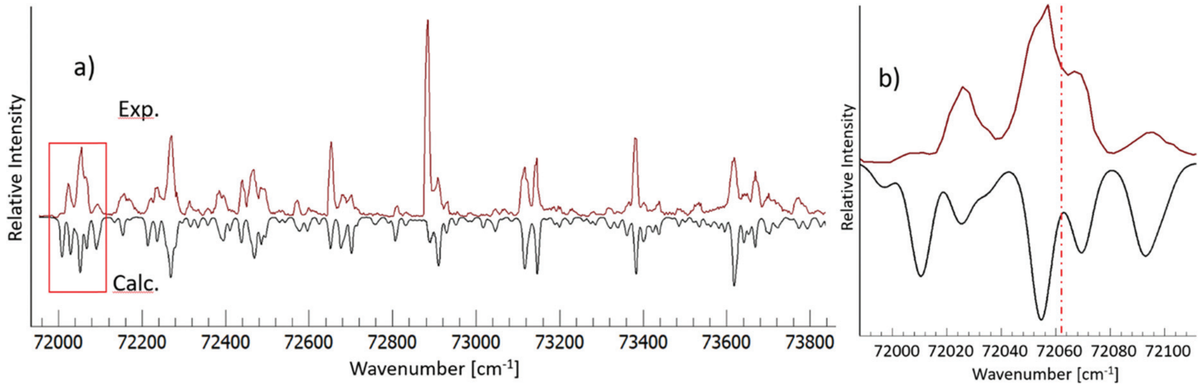

Fig. 4 Simulation of I_2 coincidence ion pair production spectra in the excitation region of 71 960–73 840 cm^{-1}. (a) Experimental spectrum on top in red and calculated spectrum on the bottom in black; the latter is formed as a result of a combination of Gaussian line widths of 8 cm^{-1} and Lorentzian line widths of 2 cm^{-1} (see main text) for a vibrational temperature of T = 40 K. (b) A magnified spectrum in the ion pair threshold energy region. Red broken line shows the ion pair threshold value (72 062.4 ± 0.5 cm^{-1}).

A good fit to the experimentally determined relative intensities in the 44.3 V cm^{-1} and 17.7 V cm^{-1} cipp spectra in the 72 015–72 080 cm^{-1} region was achieved when the spectral simulations were carried out with or without including transitions to the lowest 20 J' rotational energy levels, as shown in Fig. 5. Thus, by assigning the cutoff energy in the 17.7 V cm^{-1} cipp spectrum to the energy of the J' = 20 levels of the 7pσ(1/2) (ν' = 3) state, a value of α = −5.5 ± 0.2 cm^{-1} was obtained for the I_2 cipp process.

This observed field dependence is markedly different from what we saw in the F_2 cipp experiments, where the rotational energy resolution allowed us to directly observe how the individual rotational lines exhibited energy-dependent Stark shift, with the α value ranging from −0.96 cm^{-1} at threshold to −1.7 cm^{-1} at the high end of the studied photon energy range.

IV. Discussion

As the excitation energy closes in on the ionization potential of molecules, discreet rotational and vibrational spectra structures can be difficult to obtain by spectroscopic means. This can be partly due to increasing overlap of spectral features in association with larger density of states as the energy increases, and partly due to enhanced line broadening in association with shorter lifetime of states as the number of decay pathways increase with energy. The nature of the coincidence ion pair detection using high-resolution synchrotron radiation in conjunction with a supersonic molecular beam source bypasses some of these problems. First, the technique allows a distinction between direct ion and ion pair formation and offers very low background noise, due to the coincidence detection. Second, the jet-cooling reduces the number of observable rotational and vibrational excitations and therefore lowers overlap of spectral features. Third, in addition to a photon absorption, a crossing from the excited states to ion-pair states is involved. Thus, the latter step acts selectively to detect only spectra of Rydberg states with non-zero probabilities for transfer to the ion-pair states.

Comparison of our results with an earlier work on excitation functions for I^+ and I^- formed from photodissociation of I_2 is of particular interest.[6] The coincident ion pair detection method combined with a supersonic molecular beam inlet and a high-resolution photon source is found to greatly improve sensitivity, selectivity, and spectral resolution, allowing for detection of a many more Rydberg state transitions. The low-resolution excitation spectra in the observation region of concern were attributed to a minimum of 5 overlapping Rydberg state spectra. Three of these spectra were assigned to transitions to $[\sigma_g{}^2\pi_u{}^4\pi_g{}^3\sigma_u,\ {}^2\Pi_{3/2u}]$ npπ Rydberg states for n = 9, 10, and 11 whereas others were left unassigned. Those analyses were based on quantum defect calculations and spectral simulations as well as on an analogy to corresponding spectra derived for Br_2.[5] In contrast, our analysis reveals the involvement of a total of fifty Rydberg states in that spectral region.

All Rydberg states observed are of ungerade symmetry and either Ω = 0 or 1 according to selection rules. Therefore, assuming that homogeneous state interactions ($\Delta\Omega$ = 0) and conservation of the symmetry (u ↔ u) hold for the Rydberg to ion-pair state transfer process, only two (D($0_u{}^+$) and γ(1_u)) of six possible ion-pair states (D($0_u{}^+$), γ(1_u), δ(2_u), E($0_g{}^+$), β(1_g), and D′(2_g)) are involved.[33] The Voigt profile line widths derived from our simulation calculations of about 9.1 cm^{-1} (see above) is close to the expected fwhm of cipp spectral peaks of about 1.2 meV/9.7 cm^{-1}, suggesting that the lifetime of the Rydberg state is not shorter than about 0.6 ps.

V. Summary and conclusions

Coincidence ion pair detection was used for photoexcitation of jet cooled I_2 molecular beam in the 71 940–74 000 cm^{-1} photon energy region. The observed peak structures were attributed to vibrational bands due to transitions from the ground state (I_2 $X^1\Sigma^+(\nu''$ = 0, 1)) to a number of Rydberg states, followed by transfer to ion-pair states above the dissociation threshold to

Table 2 (a) Vibrational band origins (ν_0^0) and vibrational constants (ω_e', $\omega_e x_e'$) for Rydberg states corresponding to electron transitions to p Rydberg orbitals which belong to series converging to the Ω = 3/2 ground state of I_2^+. (b) Vibrational band origins (ν_0^0) and vibrational constants (ω_e', $\omega_e x_e'$) for Rydberg states corresponding to electron transitions to f Rydberg orbitals which belong to series converging to the Ω = 3/2 ground state of I_2^+. (c) Vibrational band origins (ν_0^0) and vibrational constants (ω_e', $\omega_e x_e'$) for Rydberg states corresponding to electron transitions to p and f Rydberg orbitals which belong to series converging to the Ω = 1/2 ground state of I_2^+

Configuration	ν_0^0 [cm^{-1}]	ω_e' [cm^{-1}]	$\omega_e x_e'$ [cm^{-1}]	Relative intensity
(a)				
$[\sigma_g{}^2\pi_u{}^4\pi_g{}^3\sigma_u,\ {}^2\Pi_{3/2u}]\ nl\lambda$				
$9p\pi_u$	71 350[a]	241	0.8	0.50
$10p\pi_u$	72 416	240	0.6	0.10
$11p\pi_u$	73 086	240	0.6	0.10
$12p\pi_u$	73 525	240	0.6	0.30
$9p\pi_u$	71 389[a]	239	0.4	0.25
$10p\pi_u$	72 440	239	0.8	0.50
$11p\pi_u$	73 098	241	0.6	0.20
$12p\pi_u$	73 535	241	0.6	0.20
$9p\sigma_u$	71 485[a]	196	0.1	0.70
$10p\sigma_u$	72 496	206	0.2	0.40
$11p\sigma_u$	73 138	199	0.6	0.35
$12p\sigma_u$	73 563	205	0.6	0.4
$9p\sigma_u$	71 654[a]	190	0.4	0.20
$10p\sigma_u$	72 602	190	0.2	0.25
$11p\sigma_u$	73 200	190	0.4	0.2
$12p\sigma_u$	73 608	190	0.6	0.2
(b)				
$[\sigma_g{}^2\pi_u{}^4\pi_g{}^3\sigma_u,\ {}^2\Pi_{3/2u}]\ nl\lambda$				
$7f\pi_u$	72 000[a]	242	0.6	0.3
$8f\pi_u$	72 815	239	0.6	0.25
$9f\pi_u$	73 341	240	0.6	0.1
$10f\pi_u$	73 705	—	—	—
$7f\delta_u$	72 035	230	0.2	0.8
$8f\delta_u$	72 839	231	0.6	0.4
$9f\delta_u$	73 360	231	0.6	0.2
$10f\delta_u$	73 719	—	—	—
$7f\sigma_u$	72 054	217	0.5	0.8
$8f\sigma_u$	72 850	215	0.6	0.4
$9f\sigma_u$	73 368	216	0.6	0.2
$10f\sigma_u$	73 724	—	—	—
$7f\pi_u$	72 135	224	0.8	0.23
$8f\pi_u$	72 901	223	0.8	0.2
$9f\pi_u$	73 403	222	0.6	0.5
$10f\pi_u$	73 748	—	—	—
$7f\delta_u$	72 155	237	0.2	0.8
$8f\delta_u$	72 914	238	0.2	0.4
$9f\delta_u$	73 409	239	0.6	0.3
$10f\delta_u$	73 750	—	—	—
$7f\sigma_u$	72 175	214	0.5	0.4
$8f\sigma_u$	72 930	216	0.6	0.35
$9f\sigma_u$	73 422	218	0.3	0.2
$10f\sigma_u$	73 766	—	—	—
(c)				
$[\sigma_g{}^2\pi_u{}^4\pi_g{}^3\sigma_u,\ {}^2\Pi_{1/2u}]\ nl\lambda$				
$7p\pi_u$	70 930[a]	238	0.9	0.50
$7p\pi_u$	71 085[a]	237	0.8	0.35
$7p\sigma_u$	71 449[a]	196	0.4	0.40
$7p\sigma_u$	72 096	190	0.8	0.25
$5f\pi_u$	73 319	238	0.6	0.2
$5f\delta_u$	73 438	231	0.6	0.5
$5f\sigma_u$	73 502	216	0.6	0.2
$5f\pi_u$	73 773	—	—	—
$5f\delta_u$	73 901	—	—	—
$5f\sigma_u$	73 912	—	—	—

[a] Based on simulation of spectra.

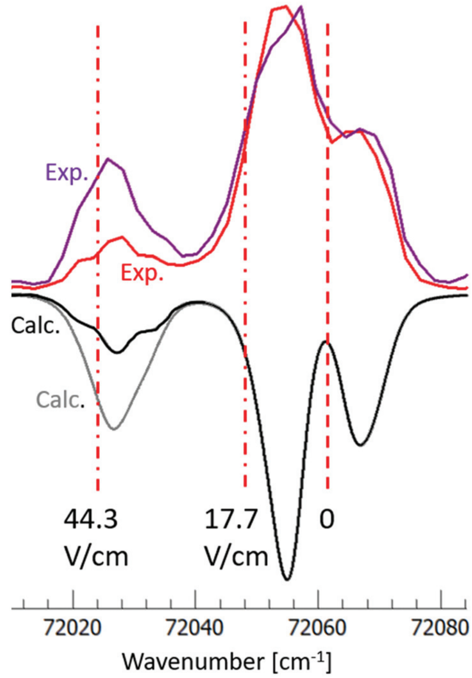

Fig. 5 Simulation of the I_2 coincidence ion pair production spectra in the excitation region of 72 015–72 080 cm^{-1}, recorded at 17.7 V cm^{-1} (red) and 44.3 V cm^{-1} (purple) electric fields; experimental spectra on top, calculated spectra inverted below. Calculated spectra are obtained without (black) and with (grey) transitions to $J' < 20$ in the 7pσ(1/2), (v' = 3) vibrational Rydberg state. The ion pair thresholds are marked by vertical broken lines for no electric field, for electric field 17.7 V cm^{-1} and for electric field 44.3 V cm^{-1}. Note that the normalization of spectral intensities is different from the inset in Fig. 1. See main text.

form the atom ion pair (I^+/I^-). Simulations of the peak structures revealed a total of fifty Rydberg states in this region and allowed the determination of spectroscopic constants (band origin, vibrational wavenumber and anharmonicity constants) for the excited states.

Transfer from Rydberg states to ion-pair states analogous to those reported here is well known for many other molecules, such as other diatomic halogens,[5–9] hydrogen halides,[34,35] and small polyatomic molecules.[36,37] In this respect, the method of coincidence ion pair detection has only been applied to the fluorine molecule.[16] Based on the present work on I_2 and our work on F_2 there is a reason to believe that coincidence ion pair production spectroscopy could be a valuable tool to explore relevant state transfer mechanisms as well as to characterize the Rydberg states involved for many other systems. Indeed, the method could be applied to number of intriguing molecular systems where Rydberg to ion-pair interactions are known to be involved. We hope that the data and interpretations presented here will produce further experimental and theoretical studies along those lines in the near future.

Conflicts of interest

There are no conflicts to declare.

Acknowledgements

B. Sz. gratefully acknowledges the support of the National Science Foundation (grant no. CHE-1665464). Experiments were performed at the DESIRS VUV beamline of the Soleil Synchrotron under proposal number 20190866 and we thank the beamline staff for their support, in particular Dr Laurent Nahon for helpful discussions in the design and preparation of the experiment. The financial support of the University Research Fund, University of Iceland and the Icelandic Research Fund (Grant No. 184693-053) is gratefully acknowledged. We are grateful to Ms Jessica De La Cruz for her help with the cipp experiments.

References

1 P. Venkateswarlu, *Can. J. Phys.*, 1970, **48**, 1055–1080.
2 R. J. Donovan, R. V. Flood, K. P. Lawley, A. J. Yencha and T. Ridley, *Chem. Phys.*, 1992, **164**, 439–450.
3 W. Huasheng, J. Ásgeirsson, Á. Kvaran, R. J. Donovan, R. V. Flood, K. P. Lawley, T. Ridley and A. J. Yencha, *J. Mol. Struct.*, 1993, **293**, 217–222.
4 Á. Kvaran, H. Wang and J. Ásgeirsson, *J. Mol. Spec.*, 1994, **163**, 541–558.
5 A. J. Yencha, D. K. Kela, R. J. Donovan, A. Hopkirk and Á. Kvaran, *Chem. Phys. Lett.*, 1990, **165**, 283–288.
6 Á. Kvaran, A. J. Yencha, D. K. Kela, R. J. Donovan and A. Hopkirk, *Chem. Phys. Lett.*, 1991, **179**, 263–267.
7 Á. Kvaran, H. Wang, G. H. Jóhannesson and A. J. Yencha, *Chem. Phys. Lett.*, 1994, **222**, 436–442.
8 Á. Kvaran, G. H. Jóhannesson and H. Wang, *Chem. Phys.*, 1996, **204**, 65–75.
9 K. P. Lawley, T. Ridley, Z. Min, P. J. Wilson, M. S. N. Alkahali and R. J. Donovan, *Chem. Phys.*, 1995, **197**, 37–50.
10 A. J. Yencha, T. Ridley, R. Maier, R. V. Flood, K. P. Lawley, R. J. Donovan and A. Hopkirk, *J. Phys. Chem.*, 1993, **97**, 4582–4588.
11 D. Kaur, A. J. Yencha, R. J. Donovan, Á. Kvaran and A. Hopkirk, *Org. Mass Spec.*, 1993, **28**, 327–334.
12 Á. Kvaran, H. Wang and G. H. Jóhannesson, *J. Phys. Chem.*, 1995, **99**, 4451–4457.
13 K. P. Lawley, T. Ridley, Z. Min, P. J. Wilson, M. S. N. Al-Kahali and R. J. Donovan, *Chem. Phys.*, 1995, **197**, 37–50.
14 J. Yang, Y. S. Hao, J. Li, C. Zhou and Y. X. Mo, *J. Chem. Phys.*, 2005, **122**, 134308.
15 J. Yang, Y. S. Hao, J. Li, C. Zhou and Y. X. Mo, *J. Chem. Phys.*, 2007, **127**, 209901.
16 K. Matthiasson, A. Kvaran, G. A. Garcia, P. Weidner and B. Sztaray, *Phys. Chem. Chem. Phys.*, 2021, **23**, 8292–8299.
17 L. Nahon, N. de Oliveira, G. A. Garcia, J. F. Gil, B. Pilette, O. Marcouille, B. Lagarde and F. Polack, *J. Synchrotron Radiat.*, 2012, **19**, 508–520.
18 G. A. Garcia, B. K. C. de Miranda, M. Tia, S. Daly and L. Nahon, *Rev. Sci. Instrum.*, 2013, **84**, 053112.
19 X. F. Tang, G. A. Garcia, J. F. Gil and L. Nahon, *Rev. Sci. Instrum.*, 2015, **86**, 123108.
20 K. Yoshino and Y. Tanaka, *J. Opt. Soc. Am.*, 1979, **69**, 159–165.
21 D. C. Morton, *Astrophys. J. Suppl. Ser.*, 2000, **130**, 403–436.
22 K. P. Huber, G. H. Herzberg, *NIST Chemistry WebBook, NIST Standard Reference Database Number 69*, ed. P. J. Linstrom and W. G. Mallard, National Institute of Standards and Technology, Gaithersburg MD, 20899.
23 G. Herzberg, *Molecular Spectra and Molecular Structure; I. Spectra of Diatomic Molecules*, Van Nostrand Reinhold Company, New York, 2nd edn, 1950, ch. VI.
24 M. C. R. Cockett, J. G. Goode, K. P. Lawley and R. J. Donovan, *J. Chem. Phys.*, 1995, **102**, 5226–5234.
25 A. Kramida, Y. Ralchenko, J. Reader and NIST ASD Team, *NIST Atomic Spectra Database (version 5.9)*, National Institute of Standards and Technology, Gaithersburg, MD, 20899.
26 PGOPHER, A Program for Simulating Rotational, Vibrational and Electronic Spectra, C. M. Western, University of Bristol, https://pgopher.chm.bris.ac.uk.
27 B. Ruscic and D. H. Bross, Active Thermochemical Tables (ATcT) values based on ver. 1.122r of the Thermochemical Network (2021); available at ATcT.anl.gov.
28 M. G. Littman, M. M. Kash and D. Kleppner, *Phys. Rev. Lett.*, 1978, **41**, 103–107.
29 E. Y. Xu, H. Helm and R. Kachru, *Phys. Rev. Lett.*, 1987, **59**, 1096–1099.
30 W. L. Glab and J. P. Hessler, *Phys. Rev. Lett.*, 1989, **62**, 1472–1475.
31 E. D. Poliakoff, J. L. Dehmer, A. C. Parr and G. E. Leroi, *Chem. Phys. Lett.*, 1984, **111**, 128–132.
32 S. T. Pratt, E. F. McCormack, J. L. Dehmer and P. M. Dehmer, *Phys. Rev. Lett.*, 1992, **68**, 584–587.
33 Á. Kvaran, S. Ó. Jónsdóttir and T. E. Thorgeirsson, *Proc. Indian Acad. Sci. (Chem. Sci.)*, 1991, **103**, 417–428.
34 A. Kvaran, K. Matthiasson and H. S. Wang, *J. Chem. Phys.*, 2009, **131**, 044324.
35 Á. Kvaran, K. Matthíasson, H. Wang, A. Bodi and E. Jonsson, *J. Chem. Phys.*, 2008, **129**, 164313.
36 K. Matthiasson, G. Koumarianou, M. X. Jiang, P. Glodic, P. C. Samartzis and A. Kvaran, *Phys. Chem. Chem. Phys.*, 2020, **22**, 4984–4992.
37 A. Kvaran, H. Wang, K. Matthiasson and A. Bodi, *J. Phys. Chem. A*, 2010, **114**, 9991–9998.